Tetracycline-Chelated Mg^{2+} Ion Initiates Helix Unwinding in Tet Repressor Induction[†,‡]

Peter Orth, Wolfram Saenger,* and Winfried Hinrichs

Institut für Kristallographie, Freie Universität Berlin, Takustrasse 6, D-14195 Berlin, Germany

Received July 14, 1998; Revised Manuscript Received October 16, 1998

ABSTRACT: The homodimeric tetracycline repressor (TetR) regulates resistance to the antibiotic tetracycline at the transcriptional level. TetR binds in the absence of Tc to palindromic operator sequences utilizing two helix−turn−helix (HTH) motifs. If the tetracycline−Mg^{2+} complex $[MgTc]^+$ enters two identical binding tunnels buried within the TetR homodimer, a conformational change takes place, and the induced $[TetR/[MgTc]^+]_2$ complex releases operator DNA. To demonstrate the contribution of Mg^{2+} to $[MgTc]^+$ binding and TetR induction, the Mg^{2+} concentration in the induced TetR homodimer was progressively reduced by addition of EDTA, resulting in two X-ray crystal structures of Mg^{2+}-free and half-occupied TetR(D). Tc remains bound to the $[MgTc]^+$-binding sites, despite the complete or partial absence of Mg^{2+}. Together with inducer-free TetR(D), the structures were refined to between 2.2 and 2.7 Å resolution and compared with fully induced TetR(D) in complex with two $[MgTc]^+$. Each inducer binding tunnel has three constituent parts, one hydrophobic and two hydrophilic ones. One of the hydrophilic contact areas binds Tc by hydrogen bonding; the hydrophobic region correctly positions Tc and partially closes the entrance to the binding tunnel; the second hydrophilic region coordinates Mg^{2+}, transduces the induction signal, and completes the process of closing the tunnel entrance. Tc confers binding specificity to TetR while Mg^{2+} is primarily responsible for induction: After binding to the imidazole Nϵ of His100, Mg^{2+} is octahedrally coordinated to the 1,3-ketoenolate group of Tc and to three water molecules. One of these waters forms a hydrogen bond to the hydroxyl group Oγ of Thr103. The induced 2.5 Å movement of Thr103 results in the partial unwinding of helix α_6, associated with a lateral shift of helices α_4 and α_9. They simultaneously close the tunnel entrance and cause the DNA-binding domains to adopt a nonbinding conformation, leading to release of operator DNA and expression of the genes responsible for resistance.

The most common resistance mechanism against tetracycline (Tc, Figure 1)[1] observed in Gram-negative bacteria is based on the active efflux of this broad-spectrum antibiotic out of the bacterial cell before it can bind to the ribosome and inhibit protein biosynthesis. The mechanism is regulated at the level of transcription by the tetracycline repressor, TetR. TetR homodimers bind with their α-helix−turn−α-helix (HTH) motifs to two nearly identical palindromic operators, *tetO*$_1$ and *tetO*$_2$, and block expression of the genes *tetA* and *tetR* which encode for the membrane-bound Tc efflux protein TetA and the repressor TetR itself (*1*). Seven variants of this resistance determinant are known, referred to as classes A−E, G, and H (*2*). The polypeptide chains of TetR contain between 207 and 219 amino acids with at least 45% sequence homology.

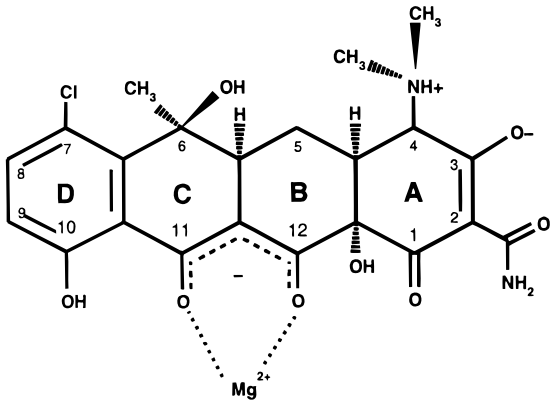

FIGURE 1: Chemical structure of the $[Mg^{7Cl}Tc]^+$ complex, which occurs under physiological conditions.

Due to its high affinity for divalent metal ions (M) under physiological pH ($K_A = 3 \times 10^4\ M^{-1}$), Tc occurs as complex $[MTc]^+$ (Figure 1) (*3, 4*). As such, it attacks the TetR/*tetO* complex by binding to TetR with a high affinity of $10^9\ M^{-1}$ (*5*), associated with a conformational change (induction) of TetR, which lowers the TetR/*tetO*-binding constant 10^2−10^3-fold upon binding of the first $[MgTc]^+$ and by an additional 10^4−10^7-fold after binding of the second $[MgTc]^+$ (*6*). This releases $[TetR/[MgTc]^+]_2$ from the operator DNA, and expression of the genes *tetR* and *tetA* can now proceed. TetA is embedded into the bacterial cytoplasmic membrane

[†] This work was supported by the Deutsche Forschungsgemeinschaft (SfB 344) and by the Fonds der Chemischen Industrie.

[‡] The coordinates for the crystal structures have been deposited in the Brookhaven Protein Data Bank (codes 1bjy, 1bjz, 1bj0).

* To whom correspondence should be addressed.

[1] Abbreviations: HTH, helix−turn−helix motif; $[MTc]^+$, complex of a divalent cation, M^{2+}, with Tc; *tetA*, gene coding for tetracycline efflux protein TetA; TetR, Tet repressor; TetR(D), Tet repressor class D; TetR(BD), chimeric construct of TetR(D) and TetR(B); ^{7Cl}Tc, 7-chlorotetracycline; Tc, tetracycline. Crystal forms: [**1**], native, inducer-free $[TetR(D)]_2$; [**2**], TetR(D) in complex with two ^{7Cl}Tc (no Mg^{2+}; $[TetR(D)/^{7Cl}Tc]_2$); [**3**], TetR(D) complexed with two ^{7Cl}Tc and one Mg^{2+} ($[TetR(D)/^{7Cl}Tc{\cdot}TetR(D)[Mg^{7Cl}Tc]^+]$); [**4**], TetR(D) complexed with two $[Mg^{7Cl}Tc]^+$ ($[TetR(D)/[Mg^{7Cl}Tc]^+]_2$).

10.1021/bi9816610 CCC: $18.00
Published on Web 12/15/1998

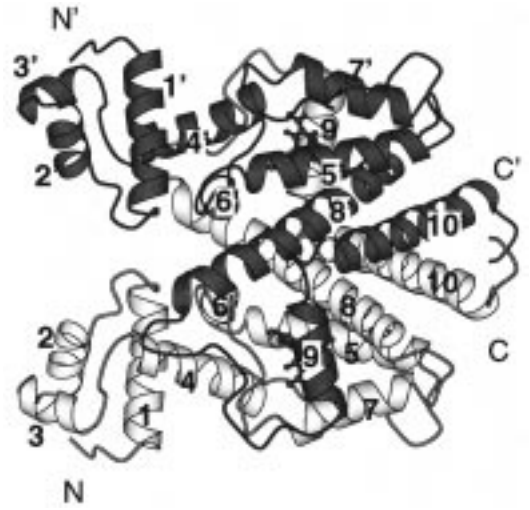

FIGURE 2: Structure of the complex [TetR(D)/[$Mg^{7Cl}Tc]^+$]$_2$, with one molecule in white and the other in gray. The TetR(D) homodimer is divided into three domains: a large, central inducer-binding core domain and two symmetrically positioned DNA-binding domains. α-Helices 2,3 and 2′,3′ form helix−turn−helix motifs. [$Mg^{7Cl}Tc]^+$ is indicated in ball-and-stick representation. This figure was generated using MOLSCRIPT (*23*).

and exports invading Tc as $[MgTc]^+$, thereby preventing the ribosomal 30S subunit from being affected because its affinity to $[MgTc]^+$ is relatively low, 10^6 M^{-1} (*7*). This way the bacterial cell achieves resistance against Tc.

The X-ray crystal structure of TetR of class D, TetR(D), shows that the homodimer has 2-fold rotational symmetry and consists of three domains: two smaller DNA-binding domains and a large core domain. The polypeptide chain of TetR(D) containing 207 residues is folded into 10 α-helices, denoted $\alpha_1-\alpha_{10}$ ($\alpha_1'-\alpha_{10}'$ for the second monomer; see Figure 2.) (*8*). The N-terminal three-helix bundles $\alpha_1-\alpha_3$ and $\alpha_1'-\alpha_3'$ form the DNA-binding domains in which α_2 and α_3 (α_2' and α_3', respectively) constitute the HTH motifs. Helices α_4 and α_4' connect the corresponding DNA-binding domains to the core domain, which is formed by helices $\alpha_5-\alpha_{10}$ and their symmetry-related counterparts. The core domain, as a unit, harbors two identical, symmetry-related and tunnel-like binding sites for $[MgTc]^+$ formed by side chains from α_5, α_6, α_7, α_8, α_8', and α_9'. Each binding tunnel has two nonequivalent openings: one of these is flexible due to a "sliding door" motion of α_9' and was identified to represent the entrance for the inducer (*9*). The other opening is more rigid and located between α_7 and the loop following α_4. After insertion into this tunnel, $[MgTc]^+$ is entirely shielded from the bulk solvent.

Relative to the TetR/*tetO* complex, binding of $[MgTc]^+$ to the TetR tunnel induces a cascade of conformational changes within the TetR dimer which culminate in an increased separation of about 5 Å between the HTH motifs, located at a distance of 33 Å from the $[MgTc]^+$-binding site. As a result, the DNA recognition helices α_3 and α_3' are now separated by 39 Å and can no longer bind to adjacent major grooves of B-DNA (with repeat of 34 Å), so that the operator DNA is released.

The inducer-free TetR(D) homodimer $[TetR(D)]_2$ [**1**] and the fully induced [TetR(D)/$[MgTc]^+]_2$ [**4**] represent two conformational extremes in binding of $[MgTc]^+$ but provide only a general insight on the specific roles of Tc and Mg^{2+} in the induction of TetR. To shed light on this process, we present two intermediate forms of TetR(D) which were obtained by treating fully induced [TetR(D)/[$Mg^{7Cl}Tc]^+]_2$ [**4**] with suitable concentrations of EDTA to wholly or partially remove Mg^{2+} from the complex. In both structures, the two binding tunnels continue to be occupied by ^{7Cl}Tc. However, while Mg^{2+} is entirely absent from the inducer binding sites in form [**2**], [TetR(D)/$^{7Cl}Tc]_2$, one of the two tunnels retains a Mg^{2+} in the other, "half-induced" structure [**3**], [TetR(D)/^{7Cl}Tc·TetR(D)/[$Mg^{7Cl}Tc]^+$]. Comparison of these four structures reveals the highly specific roles of both Tc and Mg^{2+} in the induction mechanism and identifies $[MgTc]^+$ as the actual effector molecule.

To summarize, the following denote the different repressor states discussed here: form [**1**], the inducer-free TetR(D) dimer, $[TetR(D)]_2$; form [**2**], TetR(D) dimer complexed with two ^{7Cl}Tc (no Mg^{2+}), [TetR(D)/$^{7Cl}Tc]_2$; form [**3**], TetR(D) dimer complexed with one ^{7Cl}Tc and one [$Mg^{7Cl}Tc]^+$, TetR(D)/^{7Cl}Tc·TetR(D)/[$Mg^{7Cl}Tc]^+$; and form [**4**], fully induced TetR(D) dimer, [TetR(D)/[$Mg^{7Cl}Tc]^+]_2$.

MATERIALS AND METHODS

Crystallization. TetR(D) was overproduced and purified as described (*10*). For crystallization, we used the hanging-drop vapor-diffusion method at 18 °C. Samples were prepared by mixing 5 μL of reservoir solution [1 M $(NH_4)_2SO_4$, 200 mM NaCl, and 20 mM Tris-HCl, pH 8.0] and 10 μL of the protein solutions described below. Ellipsoidal crystals typically appeared within 2−3 weeks and grew to dimensions of 0.7 mm × 0.7 mm × 0.3 mm (*11*). To obtain crystals of inducer-free TetR(D) [**1**], the protein solution contained 0.4 mM TetR(D) in 200 mM NaCl, 10 mM Tris-HCl, pH 8.0. For crystals of the fully induced [TetR(D)/[$Mg^{7Cl}Tc]^+]_2$ [**4**], 0.4 mM TetR(D), 2 mM ^{7Cl}Tc (Boehringer Mannheim), 2 mM $MgCl_2$, 200 mM NaCl, and 10 mM Tris-HCl, pH 8.0, were incubated at 30 °C for 30 min and then prepared for hanging-drop vapor diffusion experiments. All Mg^{2+} was removed from the obtained crystals by washing them for several days in a reservoir solution containing 25 mM EDTA, yielding [TetR(D)/$^{7Cl}Tc]_2$ [**2**]. To obtain TetR(D)/^{7Cl}Tc·TetR(D)/[$Mg^{7Cl}Tc]^+$ [**3**] (i.e., removing one of the two Mg^{2+} ions from [**4**]), 25 mM EDTA was added to the reservoir solution, and mixed with the protein solution in a ratio of 1:2 in the crystallization experiment, yielding an EDTA concentration in the drop of 8.3 mM, a 4-fold molar excess over the Mg^{2+} concentration.

X-ray Data Collection. All X-ray data were collected using the oscillation method (1° rotational increment) and a 180 mm diameter MAR Research imaging plate. Each data set was collected at 4 °C from a single crystal mounted in a glass capillary. X-ray sources included a rotating-anode X-ray generator (Nonius GmbH, type FR571, CuKα radiation, graphite monochromator, 0.2 × 2 mm^2 focal spot size, operated at 45 kV and 65 mA), as well as synchrotron radiation at the EMBL-outstation (beam line BW7A, DESY, Hamburg) and at the SRS Daresbury (station 9.5). The data were reduced using DENZO (*12*), scaled with SCALEPACK (*12*), and further processed with programs of the CCP4 suite (*13*). Relevant X-ray data statistics for the three data sets are summarized in Table 1.

Structure Solution and Refinement. The previously reported structure of TetR(D) in complex with ^{7Cl}Tc and Mg^{2+}

Table 1: Data Collection and Refinement Statistics

	$[TetR(D)]_2$ [**1**]	$[TetR(D)/^{7Cl}Tc]_2$ [**2**]	$TetR(D)/^{7Cl}Tc \cdot TetR(D)/[Mg^{7Cl}Tc]^+$ [**3**]
PDB entry code	1bjz	1bj0	1bjy
wavelength (Å)	0.975	0.9995	1.5418
space group	*I4₁22*	*I4₁22*	*P4₃2₁2*
unit cell at 4 °C			
$a = b$ (Å)	69.1	69.8	69.2
$c =$ (Å)	182.9	182.3	182.4
asymmetric unit	monomer	monomer	dimer
resolution limits (Å)	23.6−2.2	30.8−2.4	19.9−2.7
no. of unique reflections	10487	7958	12710
completeness (%)/redundancy	89.5/3.1	86.2/2.7	99.1/4.7
R_{sym} (%) (last 0.1 Å shell)	8.3 (36.3)	5.3 (39.7)	7.8 (22.8)
$I/\sigma(I)$ (last 0.1 Å shell)	8.19 (3.8)	12.7 (2.3)	13.3 (5.1)
R-factor/free *R*-factor (%)	23.2/29.6	24.2/32.4	20.3/26.5
rms deviations			
bond lengths (Å)	0.007	0.009	0.012
bond angles (deg)	1.21	1.33	2.58
overall isotropic *B*-factor (Å²)	57.6	68.7	46.2

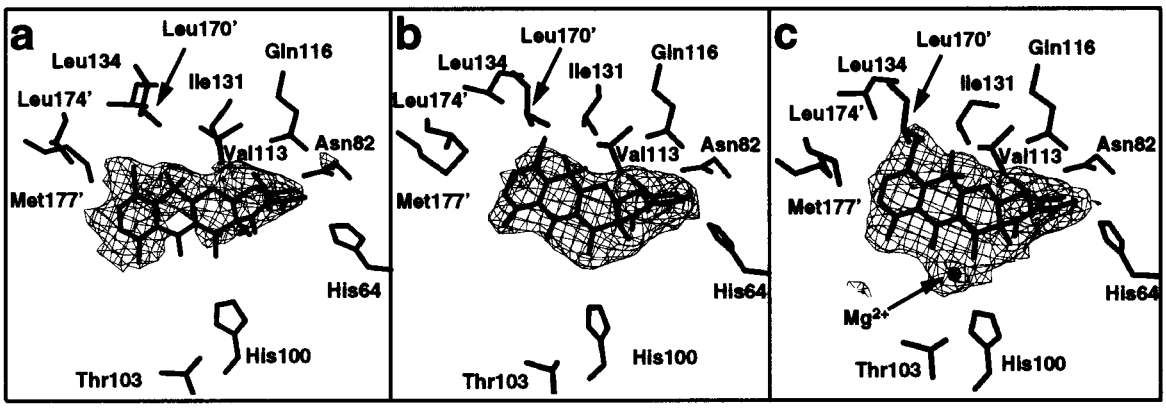

FIGURE 3: Difference electron-density maps (coefficients $F_o - F_c$, contoured at 2.5σ) showing ^{7Cl}Tc and $[Mg^{7Cl}Tc]^+$ bound to TetR(D). The maps were calculated using phases derived from models of forms **[2]** (a), **[3a]** (b), and **[3b]** (c), with inducer omitted, using the program X-plor (*15*). This figure was generated using BOBSCRIPT (*24*) and RASTER3D (*25*).

[[**4**], PDB entry code 2TCT (*11*)] served as a model in molecular replacement for crystal [**3**], using the program AMoRe (*14*). The crystals of the Mg^{2+}-free repressor/Tc complex [**2**] were sufficiently isomorphous to [**4**] so that atomic coordinates could be used directly for initial phasing. The software package X-plor V3.8 (*15*) was employed for refinement of forms [**1**], [**2**], and [**3**]. The ^{7Cl}Tc geometry was restrained according to parameters similar to those used in protein refinement (*16*). All refinement procedures were corroborated by analysis of the free *R*-factor, and model bias was reduced by following a simulated annealing protocol. The *R*-factor converged (Table 1) with alternate cycles of manual model building using the program FRODO (*17*) as well as atom positional and restrained isotropic *B*-factor refinement.

RESULTS

The Four Crystal Structures. Here we describe the characteristic features of the individual structures. Together with the previously determined structure of the induced $[TetR(D)/[Mg^{7Cl}Tc]^+]_2$ (*11*), they represent four "possible" states of complex formation between TetR, Tc, and/or $[MgTc]^+$.

(A) [1] Native or Free $[TetR(D)]_2$. This is the inducer-free form of TetR(D) with unoccupied $[MTc]^+$-binding tunnels. The space group is *I4₁22* with one TetR(D) monomer per asymmetric unit; the local dyad of the homodimeric TetR(D) coincides with a crystallographic 2-fold axis parallel to the 4-fold screw axis. The average temperature factor for main-chain and side-chain atoms is 57.6 Å². The molecular structure is very similar to that reported for a chimeric inducer-free $[TetR(BD)]_2$ (*9*) where the DNA-binding domain in TetR(D) is replaced by the corresponding polypeptide sequence of TetR(B) differing only by 10 amino acid residues. The rms deviation between main-chain atoms of these two structures is 0.66 Å. The distances between the centers of the DNA recognition helices α_3 and α_3' are similar (40.6 Å in $[TetR(D)]_2$ and 40.9 Å in $[TetR(BD)]_2$). The size of the entrance to the binding tunnel is 81 Å², ensuring the unhindered access for $[MgTc]^+$.

(B) [2] Mg^{2+}-Free, Tc-Bound TetR(D); $[TetR(D)/^{7Cl}Tc]_2$. This Tc-containing form of TetR(D) is obtained from the fully induced TetR(D) [**4**] by washing the crystals with a large excess of EDTA which leads to the complete depletion of Mg^{2+}. The space group (*I4₁22*) and the packing arrangement of TetR(D) dimers remain unchanged as compared to [**1**], but the average *B*-factor increases to 68.0 Å² compared to 57.6 Å² for crystals of [**1**]. The electron density of the bound ^{7Cl}Tc corresponds to 50% occupancy, indicating a loose association between TetR(D) and ^{7Cl}Tc (Figure 3). The entrance of the binding tunnel has an area of 72 Å², which is only a little smaller than the 81 Å² of [**1**], because helices

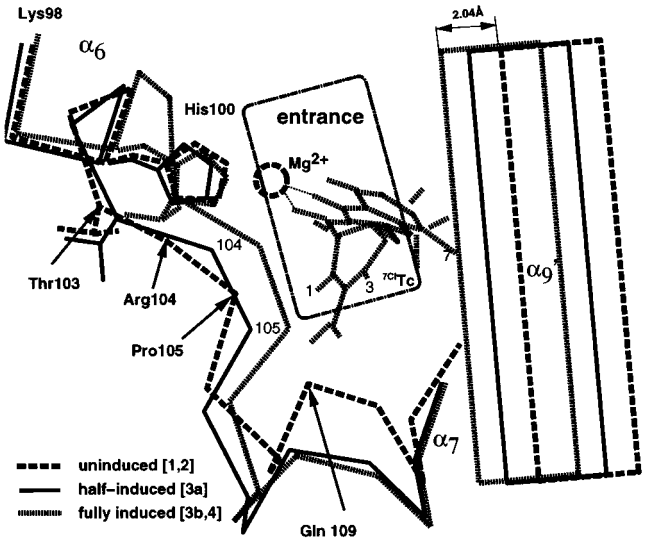

FIGURE 4: Conformational change of the entrance to the TetR(D)-binding tunnel on binding of inducer $[Mg^{7Cl}Tc]^+$. Structures: long-dashed line, [**1**] [noninduced TetR(D)]; continuous line, [**3a**] (half-induced monomer of [**3**]); and short-dashed line, [**4**] (fully induced form). During induction, helix α_9' and the loop between α_6 and α_7 are shifted toward each other, resulting in a narrowing of the entrance to the binding tunnel. Removal of Mg^{2+} from the inducer binding pocket (structures [**2**] and [**3a**]) results in the partial opening of the entrance. The opening of the binding pocket in the free TetR is marked as a point-dashed window. The view is similar as in Figure 2 to the lower binding tunnel at α_9'.

α_7 and α_9' are each shifted slightly (less than 1 Å) to accommodate ^{7Cl}Tc. The helices α_4 and α_6, which are important for induction (*9*), and the DNA-binding helices α_3 and α_3' are similar in length and orientation with respect to [**1**]. Thus, the conformation of form [**2**] is comparable to the uninduced $[TetR(D)]_2$ [**1**].

(C) [3] Partially Induced TetR(D)/^{7Cl}Tc·TetR(D)/$[Mg^{7Cl}Tc]^+$. If the molar excess of EDTA is limited to 4-fold over the Mg^{2+} concentration, the partially induced complex [**3**] crystallizes within 2 weeks. The overall crystal packing is similar to [**1**] and [**2**] as are the unit cell constants. However, the complex is now asymmetric because of conformational differences in the two inducer-binding sites. One binding site contains ^{7Cl}Tc (denoted [**3a**]), whereas the other is occupied by $[Mg^{7Cl}Tc]^+$ (denoted [**3b**]) (Figure 3). The dyad is lost, and the space group is reduced to the lower-symmetrical $P4_32_12$; the crystal asymmetric unit contains the complete TetR(D) dimer complex rather than a TetR(D) monomer as in the case of [**1**], [**2**], and [**4**].

(D) [3a] TetR(D)/^{7Cl}Tc. The conformation of the uninduced monomer [**3a**] (Figure 4, thick lines) is similar to both inducer-free [**1**] and Mg^{2+}-deficient TetR(D) [**2**], with rms deviations of main-chain atoms of 0.76 and 0.55 Å as compared to [**1**] and [**2**], respectively. These superpositions exclude the 'sliding door' α_9 at the entrance of the binding cavity of the induced, second monomer [**3b**] (see below). The overall structural differences between the Mg^{2+}-free monomer [**3a**] and both [**1**] and [**2**] (as indicated by the above rms values) are due to the flexibility of the protein near the entrance of the inducer binding tunnel in the uninduced forms [**1**] and [**2**]. This is also illustrated by the observation that ^{7Cl}Tc is located closer to the entrance of the binding tunnel in [**2**] as compared to [**3a**]. ^{7Cl}Tc rotates within the plane defined by rings B, C, and D around ring A (Figure 5), which

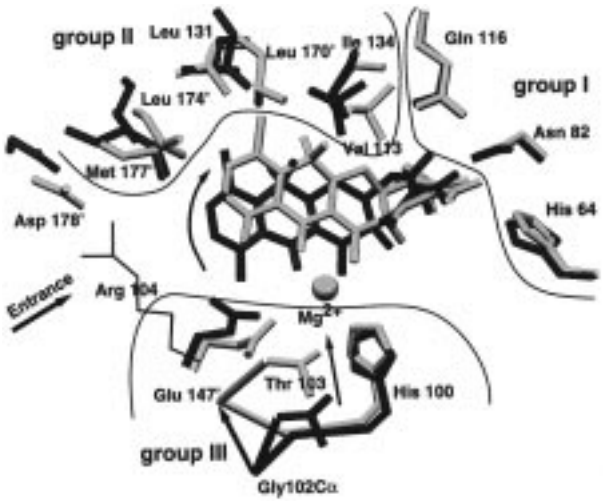

FIGURE 5: Comparison of forms [**2**] (dark) and [**4**] (light). Binding of Mg^{2+} to the inducer in the binding pocket results in C-terminal unwinding of α_6 and the rotation of bound ^{7Cl}Tc. The residues His64, Asn82, and Gln116 (group I) which serve to anchor ^{7Cl}Tc through hydrogen bonds to ring A remain largely unchanged. The side chain of Pro105 points to the upper side of the Tc-rings C and D and is omitted for clarity; for the same reason, Arg104 is shown as a thin line. This figure and Figure 6 were generated using SETOR (*26*).

Table 2: Structural Differences at the $[MgTc]^+$ Entrance

		N-terminus of α_7 (Glu107−Glu122)	shift of α_9 from uninduced to induced state (Å)
not induced	[**1**]	α-helix	0.0
not induced	[**2**]	α-helix	0.3
not induced	[**3a**]	3_{10}-helix	1.2
induced	[**3b**]	3_{10}-helix	1.9
induced	[**4**]	3_{10}-helix	2.0

is fixed by hydrogen bonds to the conserved amino acid residues His64, Asn82, Phe86, and Gln116 (Figure 4) (*8*). These side chains essentially remain unaffected in their positions. As a result, ring D of ^{7Cl}Tc is rotated away from the entrance (helix α_9) of the binding tunnel by about 1 Å in [**3a**] as compared to [**2**]. The partial closing of the entrance through hydrophobic contacts of ring D with side chains of Arg104 and Leu174′ (on α_9') leads to the partial stabilization of ^{7Cl}Tc in the binding tunnel despite the absence of Mg^{2+}. [**3a**] differs from [**1**] and [**2**] in the conformation of α-helix α_7, because the N-terminal amino acid residues, Glu107 to Tyr110, form a 3_{10}-helical turn (see Table 2). The difference between [**2**] and [**3a**] is due to the different orientation of ^{7Cl}Tc in the binding tunnel. In [**3a**], substituents of Tc-ring C form hydrophobic contacts to Val113 moving the center of α_7 away from the binding tunnel, resulting in deformation of the N-terminus of α_7, which forms a 3_{10}-helix. This deformation is also observed in the fully induced TetR(D) (*9*).

(E) [3b] TetR(D)/$[Mg^{7Cl}Tc]^+$. Compared to the uninduced monomer [**3a**], several significant structural changes are observed:

(1) In this induced monomer, helix α_9' is shifted by 0.74 Å toward both the DNA-binding domain and the loop between helices α_6 and α_7, closing the entrance of the $[MTc]^+$-binding tunnel (see Table 2). Additional hydrophobic contacts are formed between side chains of Pro105 and Met177′ to ring D of ^{7Cl}Tc.

Table 3: Temperature-Factor Distribution of ^{7Cl}Tc-Rings in Forms [**2**], [**3**], and [**4**][a]

		Tc-ring A	Tc-ring B	Tc-ring C	Tc-ring D
not induced	[**2**]	58.2	60.5	62.0	60.7
not induced	[**3a**]	53.9	61.5	71.8	76.7
induced	[**3b**]	34.5	37.6	42.4	45.4
induced	[**4**]	19.1	18.4	23.6	26.6

[a] The average temperature-factor B (Å^2) of each ^{7Cl}Tc-ring was calculated using the six constituent carbon atoms.

(2) In [**3a**], the two-turn helix α_6 is formed by the oligopeptide segment Gly96 to Gly102, as also observed in form [**1**] and the Mg^{2+}-deficient form [**2**]. In the induced monomer [**3b**], Mg^{2+} coordination is observed as in [**4**], including the unwinding of the C-terminal turn of α_6 for β-turn type II formation by residues 100−103. As a consequence, the peptide bond plane formed by Leu101 and Gly102 is rotated by 180° around the Cα−C bond of Leu101. The main-chain dihedral angles of Leu101 and Gly102 are (−46°, −45°; −79°, 11°) and (−50°, 132°; 80°, −2°) in [**3a**] and [**3b**], respectively.

(3) This conformational change of α_6 permits movement of helix α_4 of [**3b**] toward α_6 and results in a decreased separation of the DNA recognition helices α_3 and α_3' (39.9 Å) in comparison to [**1**] and [**2**].

(4) The higher mobility of ^{7Cl}Tc due to absence of Mg^{2+} near the center of the inducer-binding tunnel in [**2**] and [**3a**] as compared to [**3b**] and [**4**] is shown by an increase of the *B*-factors from ^{7Cl}Tc-rings A−D (see Table 3).

(F) [4] The Fully Induced [TetR(D)/[Mg^{7Cl}Tc]$^+$]$_2$. As in [**1**] and [**2**], crystal form [**4**] exhibits space group $I4_122$ with one monomer per asymmetric unit. [Mg^{7Cl}Tc]$^+$ is held in position in the binding tunnel by a network of hydrogen bonds and hydrophobic contacts, as described (*11*). The size of the entrance to the binding tunnel is smallest in this structure and is closed (area = 44 A^2), preventing the escape of [Mg^{7Cl}Tc]$^+$. The rms deviation for main-chain atoms between [**3b**] and the monomer in [**4**] is 0.32 Å (excluding the 'sliding door' α_9' from the calculation, see above), confirming the induced state of monomer [**3b**].

The 'lateral' shift of helix α_9 observed for [**3a**] relative to [**1**] and [**2**] above is yet more pronounced in [**4**]—the difference between the former two amounting to a mere 60% of the total shift of 2.04 Å observed for [**4**] (see Figure 4). The distance between the HTH motifs is 39.6 Å, similarly showing a decrease as compared to the uninduced [**1**] and [**2**] and half-induced [**3**] structures.

Invariant Features of TetR(D). Besides the [MgTc]$^+$-mediated conformational changes, some invariant features in all four structures should be noticed.

In contrast to the significant structural flexibility observed for the [Mg^{7Cl}Tc]$^+$-binding tunnels during induction, the structure of the DNA-binding domains does not change. Notwithstanding this internal rigidity of the three-helix bundles (α_1−α_3), the distances separating them and their relative orientations are critical for *tetO* binding or release. The differences in the separations of the recognition helices (α_3, α_3') in the discussed structures are due to a pendulum-like motion of α_4 around the C-terminus. Strictly speaking, between free and induced TetR, α_4 is rotated by 3° according His64. The induced state [**4**] is characterized by a rigid orientation of α_4, α_4', and of the associated DNA-binding domains caused by an extended cooperative hydrogen-bonding network formed by eight H_2O molecules between α_4 and α_7, whereas the inducer-free TetR(D) has sufficiently mobile three-helix bundles for *tetO* recognition due to the variable position of α_4 (*9*).

Superposition of all four structures shows that in the core domain the four-helix bundle (α_8, α_{10} and α_8', α_{10}') and α_5, α_5' form a rigid scaffold for [MgTc]$^+$ anchoring (*9*). The similarity of this feature is indicated by Leu204 of the C-terminal loop adjacent to α_{10}. The main chain torsion angles of this residue are at the borderline of the allowed region in all previously observed TetR(D) structures, but the side chain is well-defined in the electron density maps.

At the "far end" of the [MgTc]$^+$-binding tunnel, where Tc-ring A is tightly bound by hydrogen bonds to side chains His64, Asn82, Phe86, and Gln116, a second opening was located between α_7 and the loop following α_4. This rigid opening was termed as open backdoor for water release during inducer insertion into the binding tunnel (*9*) and shows no significant conformational changes in all four structures.

DISCUSSION

In the TetR(D) homodimer, the two [MTc]$^+$-binding tunnels are separated by about 25 Å, and each is again separated from the respective DNA recognition helices by roughly 33 Å. There is thus no direct interaction between the inducer-binding sites themselves or between the binding sites and the more distant DNA-binding domains. Modes of communication between these entities and the proposed step-by-step model for the mechanism of conformational changes required for induction will be discussed by comparison of the four crystal structures of TetR(D) spanning the range from the inducer-free to the induced complex.

As Tc occurs under physiological pH only as [MTc]$^+$ complex (*3*), the forms [**2**] and [**3**] are biologically not relevant but, nevertheless, of crucial importance in analyzing the structural properties of TetR(D) in different states of ^{7Cl}Tc and/or [Mg^{7Cl}Tc]$^+$ complexation and consequently in rationalizing the steps sequentially leading to complete induction.

Binding of Tc to TetR(D). The entrance to the [MTc]$^+$-binding tunnel is located between helix α_9' and the interhelical loops $\alpha_6 \cap \alpha_7$ and $\alpha_8' \cap \alpha_9'$ (*9*). In [**1**], the entrance is sufficiently large for the inducer [Mg^{7Cl}Tc]$^+$ to enter with Tc-ring A head-on to ensure recognition with TetR(D). Within the binding tunnel, the inducer forms site-specific contacts to charged, hydrophilic, and hydrophobic amino acid side chains of TetR(D). These may be divided into three categories, all of which have specific functions for inducer binding and TetR(D) induction (see Figure 5):

(1) Group I is located at the far end of the binding tunnel constituted by the conserved amino acids His64, Asn82, Phe86, and Gln116, whose side chains form hydrogen bonds to functional groups of Tc ring A.

(2) Group II is the hydrophobic region, coated by type-conserved Val113, Leu131, Ile134, Leu170′, Leu174′, and Met177′, exclusively involved in nonpolar van der Waals contacts to the hydrophobic part of [Mg^{7Cl}Tc]$^+$ with substituents at positions 6−9 and the corresponding framework of Tc-rings C and D.

(3) Group III includes side chains of conserved His100, Thr103, and Glu147′, all involved in direct or water-mediated Mg^{2+} coordination.

The Specific Function of Tc during Induction. A comparison of the inducer-free TetR(D) [**1**] and the Mg^{2+}-free TetR(D)/^{7Cl}Tc complexes [**2**] and [**3a**] allows the specific role of Tc to be investigated, without interference from the complexing metal ion. Clearly, the hydrogen bonds of group I amino acids would be the first to form, after $[MTc]^+$ has entered the binding tunnel. The relative positions of these residues remain essentially unchanged, whether Tc is present or not (Figure 5). Together with the hydrophobic contacts (group II), which guide the Tc to its final position, they serve to recognize and tightly bind the inducer to the binding tunnel.

While the hydrogen bonds and hydrophobic contacts are formed, the protein segments surrounding the hydrophobic part of Tc adapt to accommodate and lock the Tc into position. The movement of the group II residues induces a lateral shift of helix α_9' and of the loop connecting α_6 and α_7. As both helix α_9' and the interhelical loop between α_6 and α_7 form part of the entrance of the binding tunnel, the hydrophobic contacts serve to partially close the entrance, preventing the Tc from leaving the binding tunnel.

Except for the strictly conserved Leu170′, the hydrophobic group II amino acids are only type-conserved in the different classes of TetR. This agrees with the relative nonspecific nature of hydrophobic contacts allowing Tc analogues with modified hydrophobic regions to be recognized by TetR and to support induction (*18, 19*).

Comparison of the orientations of ^{7Cl}Tc in forms [**2**], [**3**], and [**4**] shows that the antibiotic occupies two positions (see Figure 5): an "intermediate" position observed in [**2**] and an "inducing" position seen in forms [**3a,b**] and [**4**]. The two positions differ in rotation of ^{7Cl}Tc around ring A, which is tightly bound by hydrogen bonds to group I amino acid side chains found in almost unchanged positions. In the "intermediate" position, the long axis of ^{7Cl}Tc points toward the "entrance" and a simple translation parallel to this axis would cause ^{7Cl}Tc to leave the binding cavity.

An "intermediate"-like position of the Tc framework was identified in the crystal structure analysis of TetR(D) in complex with a 9-(*N*,*N*-dimethylglycylamido)-substituted Tc analogue (*20*). This bulky substituent leads to a 10-fold decrease of the association constant to TetR (*19*). The crystal structure shows that steric hindrance at the entrance and interference with the "sliding door" function of α_9' by the 9-glycyl moiety lead to the "intermediate position" of the Tc framework. As a result, the Mg^{2+} ion binding to TetR is impaired, because the Mg^{2+}-coordination octahedron is not recognized with the same hydrogen bonding pattern in the binding tunnel of TetR like the fully induced [**4**] (*20*). Consequently, in the absence of Mg^{2+} ions, the binding constant to TetR is about 2 orders of magnitude higher for 9-amino derivatives of Tc ($K_A \approx 10^7\ M^{-1}$) than for 7HTc (*19*).

The Specific Function of Mg^{2+} during Induction. The specific role of Mg^{2+} in the process of induction is illustrated by comparing the uninduced [TetR(D)/^{7Cl}Tc] structures [**2**] and [**3a**] with the induced [TetR(D)/$[MgTc]^+$] structures [**3b**] and [**4**]. Three strictly conserved amino acid residues of TetR(D) are involved in binding Mg^{2+}: His100, Thr103, and Glu147′. Of these, only Nϵ of His100 is involved in the first, octahedral coordination sphere of Mg^{2+}, the other ligands being provided by three water molecules and the chelating 1,3-ketoenolate of Tc (Figures 1 and 6).

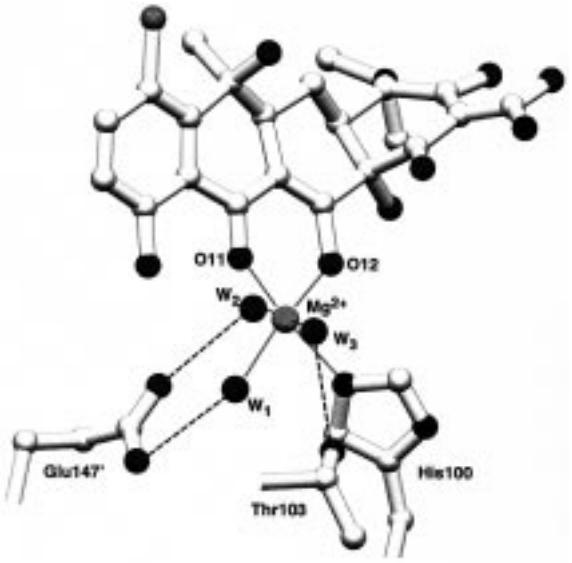

FIGURE 6: Octahedral Mg^{2+}-coordination sphere in the inducer binding pocket. The ligands are supplied by the two ^{7Cl}Tc atoms O11 and O12 of the 1,3-ketoenolate, NϵHis100, and three water molecules W1, W2, and W3. The coordination bonds to Mg^{2+} are shown as dotted lines; hydrogen bonds to the three water molecules are dashed lines.

A hydrogen-bonding network of the three water ligands of Mg^{2+} is established with amino acid side chains of Thr103 and Glu147′. As part of this recognition process, the carboxylate group of Glu147′ is rotated by 90°, forming hydrogen bonds to two of the Mg^{2+}-coordinated water molecules. The flexibility of the Glu147′ side chain allows this rotation to occur without a significant change in the position of the protein backbone (Figure 5). In hydrogen bonding to the remaining third water molecule, the side chain of Thr103 dramatically shifts by 2.5 Å, forcing the backbone between Gly102 and Arg104 to move by 3.2 Å. Thr103 is the first amino acid residue C-terminal to helix α_6. Its shift induces a tension of helix α_6 resulting in unwinding the C-terminal part of α_6 to adopt a β-turn conformation (residues His100 to Thr103). The amino acid residues of helix α_6 itself are in van der Waals contact with those of α_4 which is responsible for positioning of the DNA-binding domain. The C-terminal shortening of α_6 causes α_4 to perform a pendulum-like motion around its C-terminal residue, His64, thereby communicating the impulse of induction to the DNA-binding domains.

The movement of Thr103 (Figure 5) is accompanied by the neighboring amino acids Arg104 and Pro105, which are conserved in all TetR classes with the exception of Ser104 in TetR(E). These amino acids are part of the interhelical turn between α_6 and α_7. The functional importance of the Thr103 side chain is shown by noninducible mutants (*21*, *22*) where Thr103 is substituted by Ala, Ile, and Lys. In addition to the hydrogen bonding to a Mg^{2+}-coordinated water ligand, Thr103Oγ stabilizes the induced β-turn by a hydrogen bond to the peptide carbonyl group of His100. Pro105 as part of the hydrophobic pocket is in contact with rings C and D of ^{7Cl}Tc, which is even tightened due to the motion of Thr103 leading to a consolidation of the hydrophobic contacts and a tighter hydrophobic pocket (Figure 4,

[**3b**] and [**4**]). Arg104 in turn forms a salt bridge to the Asp178′ of helix α_9' (Figure 5), inducing this helix to move yet closer to ^{7Cl}Tc, thereby reinforcing the shift caused by the hydrophobic contacts between rings C and D to the group II amino acid residues. This completes the "sliding-door" motion of α_9' and closure of the entrance to the inducer binding tunnel (Figure 4).

Note that the position of ^{7Cl}Tc is somewhat different in the Mg^{2+}-free [**2**] compared to the other states ([**3a**], [**3b**], and [**4**]). Thus, inducer binding proceeds via two steps: First, insertion of $[MTc]^+$ into the binding tunnel results in hydrogen bonding between ^{7Cl}Tc-ring A and the group I residues, comparable to that seen in [**2**]. Second, there is a rotation of ^{7Cl}Tc around ring A (fixed by its hydrogen-bonding network) to form the hydrophobic contacts and to position the chelated Mg^{2+} appropriate for binding to the imidazole ring of His100.

Only $[MgTc]^+$ is able to trigger the mechanism of conformational changes for induction, but not the Tc molecule without the coordinated Mg^{2+} ion. This is clearly shown by the homodimeric TetR(D) in complex with one Tc and one $[MgTc]^+$. If only Tc occupies the binding tunnel, the corresponding TetR(D) monomer remains almost unchanged and is very similar to the structure of the free TetR(D). Recognition of ^{7Cl}Tc-chelated Mg^{2+} by imidazole of His100 allows Thr103Oγ to form a hydrogen bond to a water ligand of the octahedral Mg-coordination sphere initiated by rearrangements of the C-terminal turn of α_6 (*9*).

Communication between the Inducer-Binding Pockets. In the crystal packing of [**3**], statistical disorder with respect to the induced/noninduced state of the TetR(D) monomers is not observed. This is probably due to the crystal contacts of the entrance regions of neighboring TetR dimers. The entrance of an induced monomer is always next to the entrance of the noninduced half of another TetR dimer. This systematic packing is probably a more stable arrangement than the alternative statistical disorder. These crystal packing contacts are probably a reason for the observed different positioning of α_9' in the uninduced complexes [**2**] and [**3a**] (see Figure 4).

The existence of the half-induced TetR(D) with one monomer in the induced, $[MgTc]^+$-bound conformation and the other monomer in the uninduced, Tc-bound conformation is in agreement with fluorescence−spectroscopic experiments, where no detectable cooperativity was observed using free TetR (*18, 19*). According to our data, conformational changes induced by $[MgTc]^+$ coordination in one binding tunnel of the TetR core caused no structural variations in the other one. In contrast, an apparent discrepancy arises from thermodynamic analysis of inducer binding to the TetR/*tetO* complex, where cooperativity was observed. Binding of the first inducer already reduces the affinity of TetR to operator by about 3 orders of magnitude. This is sufficient for significant operator release upon binding of the first inducer (*6*) and initiates the resistance mechanism at subinhibitorical concentrations of Tc (*2*). The second $[MgTc]^+$ lowers the TetR/*tetO*-binding constant by additional 10^4-10^7-fold. The observed cooperativity can be assigned to the DNA-binding domains which are operator-bound, whereas in free TetR they are independent.

After inducer binding to the TetR/operator complex, conformational rearrangements stabilize the orientations of the DNA-binding domains in the 39.6 Å separation of the recognition helices $\alpha3$ and $\alpha3'$, abolishing the affinity for operator DNA. The observed interrelation of inducer binding and induction of the TetR/operator complex is an effect of the stepwise changed mobility of the two DNA-binding domains caused by inducer binding. If only one $[MgTc]^+$ is bound to the TetR(D) dimer, the corresponding HTH motif is forced into the induced orientation and the operator recognition is significantly weakened. The noninduced monomer is still able to vary its relative position to the other, fixed DNA-binding domain and compensates the half-induced situation to some extent.

Movement of the DNA-Binding Domains. In the four structures, the separation of the recognition helices α_3, α_3' varies between 39.6 Å in the induced state [**4**] and 40.6 Å in the uninduced conformation [**1**]. The apparent ambiguity with respect to the assumed separation of 34 Å for binding to the major groove of the operator DNA was discussed recently (*9*). In [**4**], both DNA-binding domains ($\alpha_1-\alpha_3$) are positioned by the orientation of α_4. After $[MgTc]^+$ binding, the β-turn formation C-terminal to α_6 forces α_4 into a specific position, which is fixed by an extending network of water-mediated hydrogen bonds connecting the inducer binding site to several peptide carbonyl groups of α_4. This ordered water arrangement was not found in all uninduced structures. The DNA-binding domains are assumed to be mobile for operator recognition and separated by their equal charge and probably also crystal packing contacts (*9*).

ACKNOWLEDGMENT

We are grateful for synchrotron beam time allocations at both the SRS, Daresbury, and the EMBL-outstation at DESY, Hamburg. Our particular thanks are to Heike Roscher for preparation of TetR(D) and to Wolf-Dieter Schubert for critical reading of the manuscript.

REFERENCES

1. Hillen, W., and Berens, C. (1994) *Annu. Rev. Microbiol. 48*, 345−369.
2. Schnappinger, D., and Hillen, W. (1996) *Arch. Microbiol. 165*, 359−369.
3. Jogun, H. J., and Stezowski, J. J. (1976) *J. Am. Chem. Soc. 98*, 6018−6026.
4. Takahashi, M., Altschmied, L., and Hillen, W. (1986) *J. Mol. Biol. 187*, 341−348.
5. Takahashi, M., Degenkolb, J., and Hillen, W. (1991) *Anal. Biochem. 199*, 197−202.
6. Lederer, T., Takahashi, M., and Hillen, W. (1995) *Anal. Biochem. 232*, 190−196.
7. Epe, B., and Woolley, P. (1984) *EMBO J. 3*, 121−126.
8. Hinrichs, W., Kisker, C., Düvel, M., Müller, A., Tovar, K., Hillen, W., and Saenger, W. (1994) *Science 264*, 418−420.
9. Orth, P., Cordes, F., Schnappinger, D., Hillen, W., Saenger, W., and Hinrichs, W. (1998) *J. Mol. Biol. 279*, 439−447.
10. Ettner, N., Müller, G., Berens, Ch., Backes, H., Schnappinger, D., Schreppel, T., Pfleiderer, K., and Hillen, W. (1996) *J. Chromatogr., Sect. A 742*, 95−105.
11. Kisker, C., Hinrichs, W., Tovar, K., Hillen, W., and Saenger, W. (1995) *J. Mol. Biol. 247*, 260−280.
12. Otwinowski, Z., and Minor, W. (1997) *Methods Enzymol. 276*, 307−326.
13. CCP4 (1994) *Acta Crystallogr. D50*, 760−763.
14. Navaza, J., and Saludjian, P. (1997) *Methods Enzymol. 276*, 581−593.
15. Brünger, T. A. (1996) *X-PLOR Manual version 3.843*, Yale University Press, New Haven, CT.

16. Engh, R., and Huber, R. (1991) *Acta Crystallogr. A47*, 392−400.
17. Jones, A. T. (1985) *Methods Enzymol.*, 157−171.
18. Degenkolb, J., Takahashi, M., Ellestad, G. A., and Hillen, W. (1991) *Antimicrob. Agents Chemother. 35*, 1591−1595.
19. Lederer, T., Kintrup, M., Takahashi, M., Sum, P.-E., Ellestad, G. A., and Hillen, W. (1996) *Biochemistry 35*, 7439−7446.
20. Orth, P., Schnappinger, D., Sum, P.-E., Ellestad, G. A., Hillen, W., Saenger, W., and Hinrichs, W. (1998) *J. Mol. Biol.* (in press).
21. Smith, L. D., and Bertrand, K. P. (1988) *J. Mol. Biol. 203*, 949−959.
22. Müller, G., Hecht, B., Helbl, V., Hinrichs, W., Saenger, W., and Hillen, W. (1995) *Nat. Struct. Biol. 2*, 693−703.
23. Kraulis, P. J. (1991) *J. Appl. Crystallogr. 24*, 946−950.
24. Esnouf, R. M. (1997) *J. Mol. Graphics 15*, 133−138.
25. Merritt, E. A., and Murphy, M. E. P. (1994) *Acta Crystallogr. D50*, 869−873.
26. Evans, S. V. (1993) *J. Mol. Graphics 11*, 134−138.

BI9816610